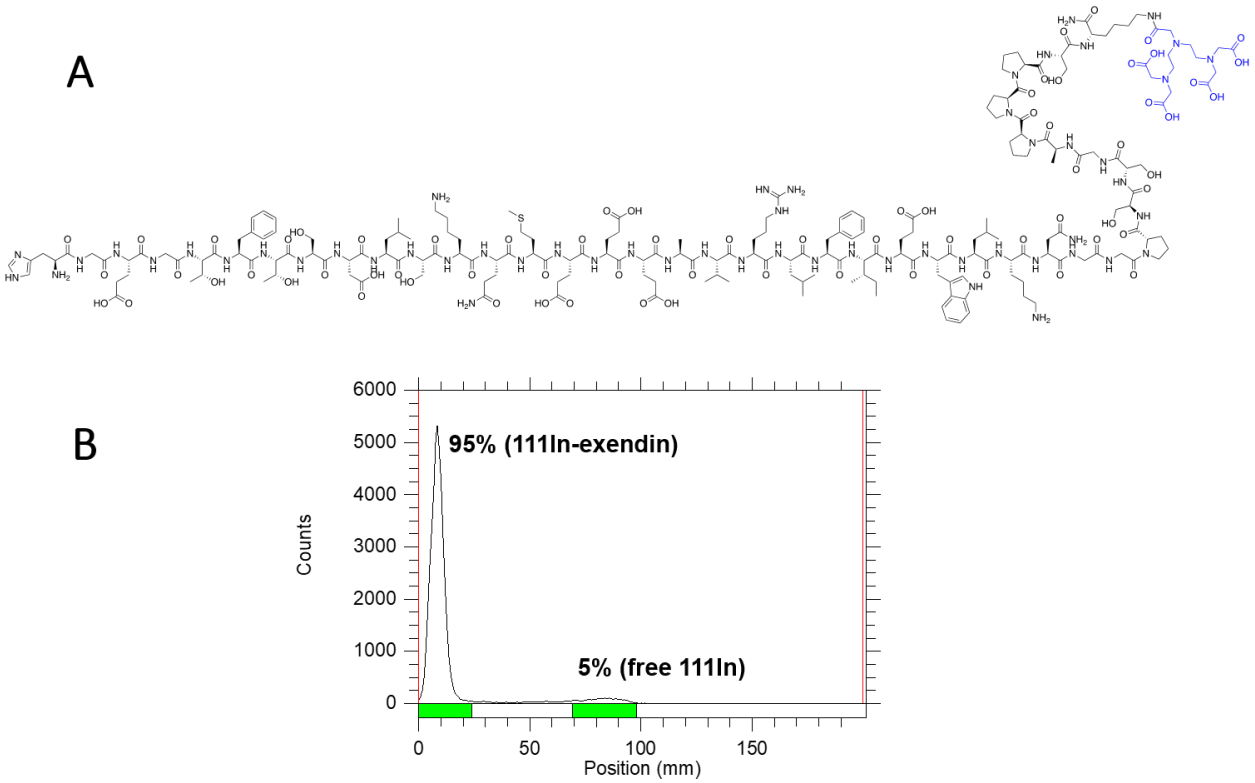

Supplemental Figure 1. Preparation of radiolabeled exendin conjugate (Lys^{40}(^{111}In-DTPA) exendin-4). (A) Structure of Lys^{40}(^{111}In-DTPA) - (DTPA)] exendin-4. Wild-type exendin-4 (H-HGEGTFTSDLSKQMEEEAVRLFIEWLKNGGPSSGAPPPS-NH_2), single mutant exendin-4 (H-HGEGTFTSDLSKQ**X**EEEAVRLFIEWLKNGGPSSGAPPPS-NH_2) where **X** is the non-natural amino acid azidohomoalanine (AHA) for fluorescent labeling, and Lys^{40}(^{111}In-DTPA) exendin-4 (H-HGEGTFTSDLSKQMEEEAVRLFIEWLKNGGPSSGAPPPS-Lys(DTPA)-NH2) where DTPA is diethylenetriaminepentaacetic acid for ^{111}In radiolabeling, were custom synthesized from Innopep (San Diego, CA). Preparation and characterization of AlexaFluor 647 single mutant exendin (hereon referred to as 647-exendin) and Cy7 single mutant exendin (hereon referred to as Cy7-exendin) was performed following previously published protocols(*1,2*). The DTPA was conjugated to the ε-amino group of the lysine (K40). ^{111}In-Cl_3 for radiolabeling was obtained from Nuclear Diagnostic Products (Rockaway, NJ). All radioactive materials were handled and disposed following MKSCC standard operating procedures. Lys^{40}(^{111}In-DTPA) exendin-4 (1 µg in DMSO) was added to 848 µL of 0.1 M MES (2-(N-morpholino)ethanesulphonic acid) buffer, pH 5.5. with 1.31 mCi ^{111}In-Cl_3 (48 MBq, 50 µL), resulting in a total volume of 900 µL of the reaction mixture, maintained at a pH of 5.5. The reaction mixture was vortexed at room temperature (20° C) for 30 min. (B) Instant thin layer chromatography (iTLC) of reaction mixture shows >95% exendin radiolabeling. Formation of Lys^{40}(^{111}In-DTPA) exendin (hereon referred to as 111In-exendin) was monitored using an instant thin-layer chromatography (iTLC) using silica gel plates

from Sigma-Aldrich (Milwaukee, WI). 40 mM EDTA at pH 5.5 was used as the mobile phase, and purity/yield was assessed based on the retention distance (Rf). Under these conditions, >95% radiolabeling was achieved and the quality control was performed using instant thin-layer chromatography (iTLC).

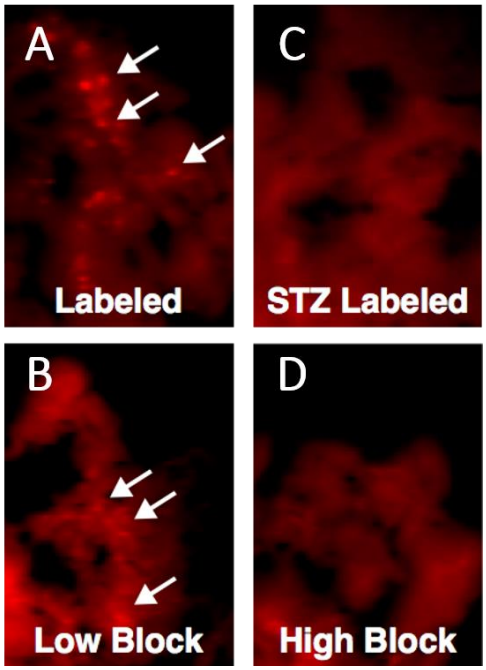

Supplemental Figure 2. Whole organ fluorescence imaging of healthy 647-exendin mice showing presence of punctate signal from islets in (A) label pancreas and (B) low block pancreas, but not in (C) STZ-diabetic labeled pancreas and (D) high block pancreas.

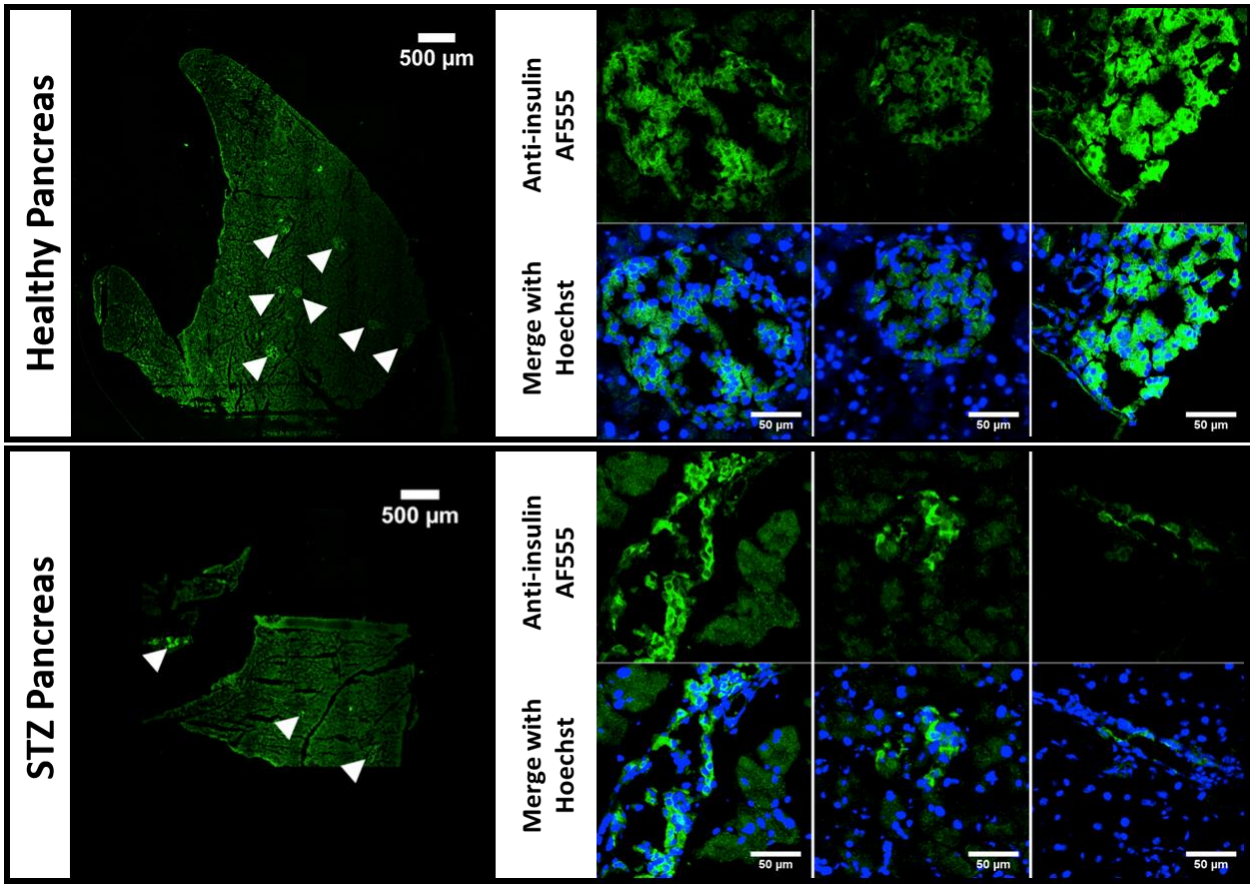

Supplemental Figure 3. Reduced insulin-expressing islets in STZ-diabetic mice. Histology slices of healthy and STZ-diabetic pancreases stained with an AF555-labeled anti-insulin antibody shows an abundance of large, insulin-positive islets (~50-200 µm) in the healthy pancreas compared to the smaller, scarce insulin-positive islets (~20-100 µm) in STZ diabetic pancreas.

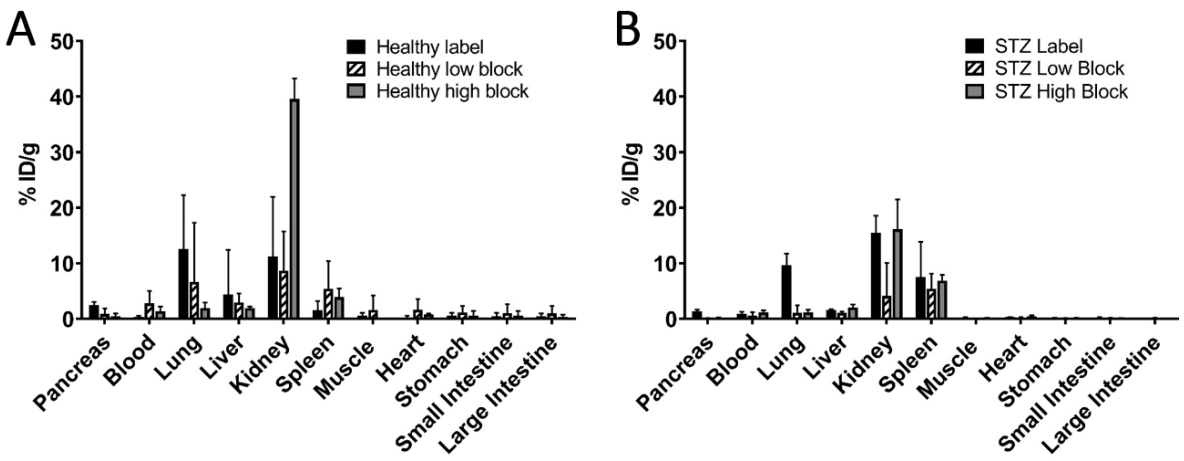

Supplemental Figure 4. Systemic accumulation of radiolabeled exendin represented by biodistribution analysis of radiolabel exendin dose in other mouse organs. Interestingly, the progressively decreasing trend in uptake in healthy pancreata was also observed in healthy and STZ-diabetic mice lungs, consistent with the localization of exendin probes in lungs due to GLP-1R expression(*3*,*4*). Since GLP-1R is also expressed in human lungs(*4*), this selective blocking strategy could provide the additional benefit of reducing clinical radiotoxicity from off-target 111In-exendin uptake in lungs.

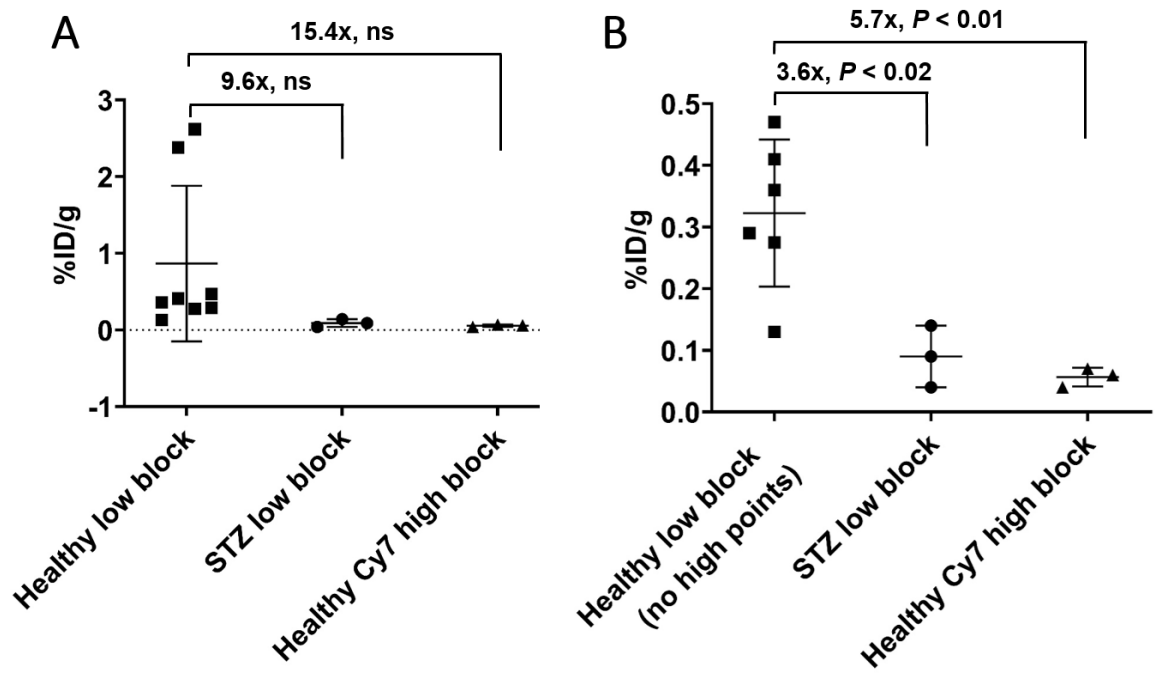

Supplemental Figure 5. 111In-exendin uptake in healthy low block compared to STZ low block and healthy Cy7-exendin high block. (A) The %ID/g of the healthy low block, though higher than STZ low block and healthy Cy7-exendin high block, is not statistically significant. This is due to the large standard deviation of the healthy low block data wherein two data points show high uptake of 111In-exendin (~2.5 %ID/g) in the pancreas, which is consistent with the expected result from blocking all exocrine pancreas but not as many β-cell GLP-1R. Since the Cy7-exendin pre-block dose was estimated to err on the side of complete exocrine blocking, the other uptake data points in healthy low block mice were ~0.3 %ID/g. This large variability precludes the data from showing statistical significance. (B) Without the two high uptake data points, the healthy low-block data is statistically higher than both STZ low block (3.6-fold, $P < 0.02$) and healthy Cy7-exendin high block (5.7-fold, $P < 0.01$), compared to 1.7-fold for label.

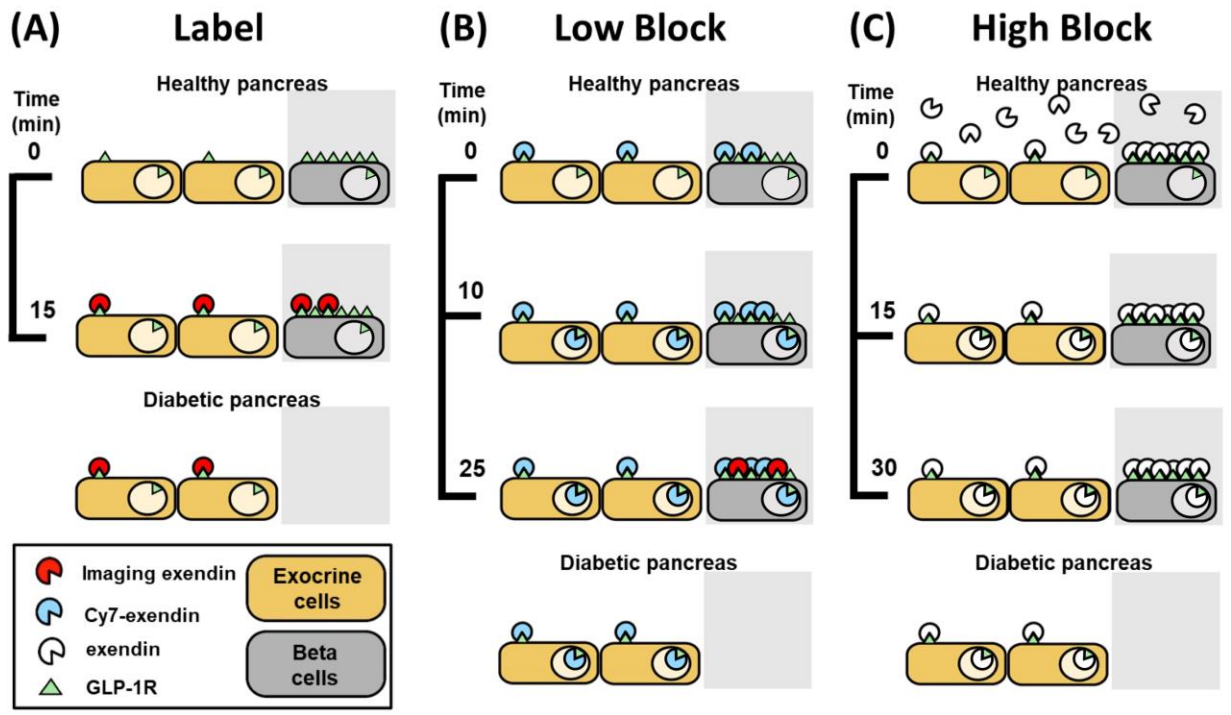

Supplemental Figure 6. Schematic detailing mechanism of selective blocking with lipophilic Cy7-exendin including internalization. (A) When an imaging dose is administered directly ('Label'), it can bind to GLP-1R on both exocrine and β-cells. This explains the higher than anticipated uptake in long-term diabetics who should lack any β-cells, complicating the use of exendin for β-cell imaging. (B) Administration of a small lipophilic pre-block dose ('Low block') provides a potential solution to this challenge by selectively blocking all exocrine GLP-1R while leaving enough β-cell GLP-1R available for binding to the imaging probe. The lipophilicity of the pre-block probe provides several advantages – first, its interaction with plasma proteins enables slower clearances, allowing it to accumulate for longer in the pancreas and block all exocrine GLP-1R as they are trafficked in and out of cells. Second, the slower diffusion prevents the blocking dose from diffusing into and blocking islets from surrounding exocrine, enhancing the selectivity of exocrine GLP-1R blocking. (C) Cold-dose blocking with unlabeled exendin (15-fold more than imaging probe) blocks all available GLP-1R, preventing any uptake of the imaging exendin, and serves as a negative control.

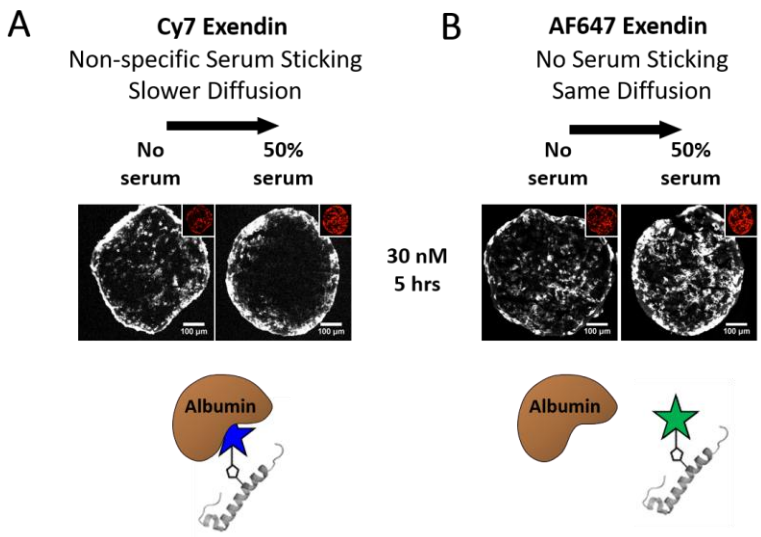

Supplemental Figure 7. Lipophilicity of Cy7-exendin enhances selective blocking of exocrine GLP-1R. (A) Diffusion of lipophilic Cy7-exendin and (B) hydrophilic 647-exendin in GLP-1R positive (inset) spheroids. Theoretical estimates postulate 3-fold higher delivery and uptake in islets compared to exocrine pancreas, due to 3-fold better blood surface area (500 cm^2/cm^3 in islets vs 180 cm^2/cm^3 in exocrine), but ex vivo histology shows almost 5-fold higher uptake(*5*), suggesting that diffusion of the inherently hydrophilic exendin into islets from surrounding exocrine is also a contributing factor. Hydrophilic exendin attains rapid kinetic equilibration, so binding affinity becomes the major factor that determines blocking of exocrine vs β-cell GLP-1R. However, since the binding affinity of exendin to exocrine and β-cell GLP-1R is identical, a hydrophilic exendin cannot achieve selective blocking of exocrine GLP-1R over β-cell GLP-1R. Conjugation of a lipophilic moiety could slow the diffusion of the pre-block dose from exocrine to islets due to plasma protein sticking(*2*). HEK-293 cells transfected with GLP1R-GFP(*2*) were used to grow spheroids in custom-made 384-well plates developed previously(*6*) using the hanging drop method. Details on spheroid culture, processing, and imaging conditions can be provided on request. Diffusion of Cy7-exendin (lipophilic) and 647-exendin (hydrophilic) in the presence and absence of serum proteins in 3D spheroid cultures confirmed that unlike 647-exendin, which diffused throughout the spheroid regardless of the presence or absence of serum, Cy7-exendin showed a remarkably different distribution profile. In the absence of serum, Cy7-exendin diffused throughout the spheroids, similar to 647-exendin (200-250 μm from the edge of the spheroid). However, in the presence of 50% serum, Cy7-exendin only stained the rim (50-100 μm from the edge), despite GLP-1R expression throughout the spheroid (red inset). This is consistent with non-specific sticking of the lipophilic Cy7 moiety to serum proteins, which slows the inherently fast diffusion expected from a small peptide like exendin, supporting the hypothesis that the use a lipophilic pre-block slows the diffusion of exendin from exocrine to islets, thereby enhancing the selectivity of exocrine GLP-1R blocking.

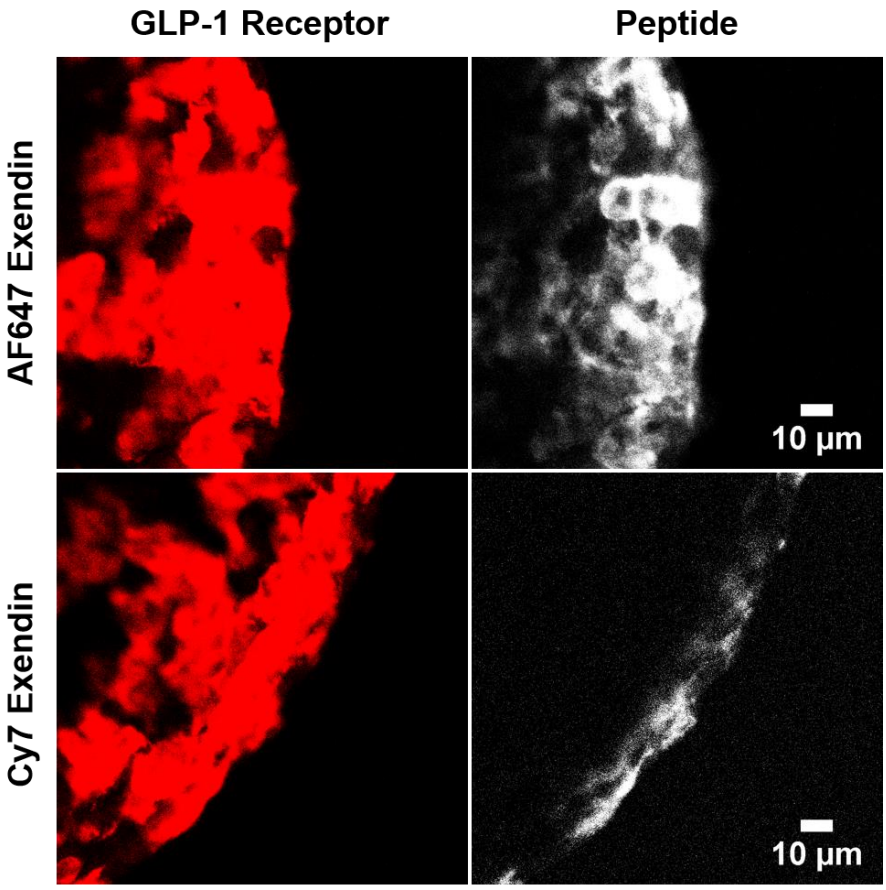

Supplemental Figure 8. High magnification confocal imaging of the edge of HEK293-GLP-1R spheroids pulsed with 10 nM (the estimated concentration of the low-block dose in the pancreas) of either hydrophilic AF647-exendin or lipophilic Cy7-exendin for 10 min (similar time scale as *in vivo* pulse) to estimate how far the peptides diffuse into tissue. Hydrophilic AF647-exendin can diffuse approximately 70 µm from the edge of the spheroid within 10 minutes in the presence of serum, equivalent to diffusing to the center of a 140 µm diameter islet, which is similar in size to mouse islets. Lipophilic Cy7-exendin however, does not diffuse beyond the first cell layer, indicating minimal exposure beyond the outer edge.

Supplemental Table 1. Specific activity of 111In-exendin injected dose.

Healthy				STZ			
Mouse	**Quantity peptide(μg)/50μL**	**Activity (μCi)**	**Specific activity (MBq)/nmol**	**Mouse**	**Quantity peptide(μg)/50μL**	**Activity (μCi)**	**Specific activity (MBq)/nmol**
Label				Label			
1	0.0021	0.87	69.9	1	0.002	0.24	20.2
2	0.0021	0.69	55.4	2	0.002	0.2	16.9
3	0.0021	0.69	55.4	3	0.002	0.22	18.6
Low block				Low block			
1	0.002	1.5	126.5	1	0.002	1.07	90.3
2	0.002	1.08	91.1	2	0.002	1.08	91.1
3	0.002	1.1	92.8	3	0.002	7.45	628.5
1	0.002	1.4	118.1	High block			
2	0.002	1.3	109.7	1	0.002	0.21	17.7
3	0.002	1.3	109.7	2	0.002	0.2	16.9
1	0.002	8.65	729.7	3	0.002	0.2	16.9
2	0.002	9.16	772.7				
3	0.002	8.2	691.8				
High block							
1	0.0021	0.63	50.6				
2	0.0021	0.71	57.0				
3	0.0021	0.64	51.4				
Cy7-exendin high block							
1	0.002	0.52	43.9				
2	0.002	0.52	43.9				
3	0.002	0.51	43.0				

References

1. Zhang L, Navaratna T, Thurber GM. A helix-stabilizing linker improves subcutaneous bioavailability of a helical peptide independent of linker lipophilicity. *Bioconjug Chem.* 2016;27:1663-1672.

2. Zhang L, Thurber GM. Quantitative impact of plasma clearance and down-regulation on GLP-1 receptor molecular imaging. *Mol Imaging Biol.* 2016;18:79-89.

3. Monazzam A, Lau J, Velikyan I, et al. Increased expression of GLP-1R in proliferating islets of men1 mice is detectable by [68Ga]Ga-DO3A-VS-Cys40-exendin-4 /PET. *Sci Rep.* 2018;8:748-748.

4. Viby N-E, Isidor MS, Buggeskov KB, Poulsen SS, Hansen JB, Kissow H. Glucagon-like peptide-1 (GLP-1) reduces mortality and improves lung function in a model of experimental obstructive lung disease in female mice. *Endocrinology.* 2013;154:4503-4511.

5. Eriksson O, Rosenström U, Selvaraju RK, Eriksson B, Velikyan I. Species differences in pancreatic binding of DO3A-VS-Cys40-Exendin4. *Acta Diabetol.* 2017;54:1039-1045.

6. Tung YC, Hsiao AY, Allen SG, Torisawa YS, Ho M, Takayama S. High-throughput 3D spheroid culture and drug testing using a 384 hanging drop array. *Analyst.* 2011;136:473-478.